Journal Pre-proof

Selective conversion of xylose to lactic acid over metal-based Lewis acid supported on γ-Al_2O_3 catalysts

Chanokporn Kosri, Sirapassorn Kiatphuengporn, Teera Butburee, Saran Youngjun, Sutarat Tongrutkaew, Kajornsak Fuangnawakij, Chakrit Yimsukanan, Narong Chanlek, Pinit Kijkhuntod, Jatuporn Wittayakun, Pongtanawat Khemthong

PII: S0920-5861(20)30270-4

DOI: https://doi.org/10.1016/j.cattod.2020.04.061

Reference: CATTOD 12840

To appear in: *Catalysis Today*

Received Date: 31 December 2019

Revised Date: 1 April 2020

Accepted Date: 30 April 2020

Please cite this article as: Kosri C, Kiatphuengporn S, Butburee T, Youngjun S, Tongrutkaew S, Fuangnawakij K, Yimsukanan C, Chanlek N, Kijkhuntod P, Wittayakun J, Khemthong P, Selective conversion of xylose to lactic acid over metal-based Lewis acid supported on γ-Al_2O_3 catalysts, *Catalysis Today* (2020), doi: https://doi.org/10.1016/j.cattod.2020.04.061

Selective conversion of xylose to lactic acid over metal-based Lewis acid supported on γ-Al_2O_3 catalysts

Chanokporn Kosri[1], Sirapassorn Kiatphuengporn[2], Teera Butburee[2], Saran Youngjun[2], Sutarat Tongrutkaew[2], Kajornsak Fuangnawakij[2], Chakrit Yimsukanan[2], Narong Chanlek[3], Pinit Kijkhuntod[3], Jatuporn Wittayakun[1,*], and Pongtanawat Khemthong[2*]

[1]School of Chemistry, Institute of Science, Suranaree University of Technology, Nakhon Ratchasima, Thailand

[2]Nanotechnology Center (NANOTEC), National Science and Technology Development Agency (NSTDA), Pathum Thani, Thailand

[3]Synchrotron Light Research Institute, Nakhon Ratchasima, Thailand

*Corresponding authors: pongtanawat@nanotec.or.th and jatuporn@g.sut.ac.th

Graphical abstract

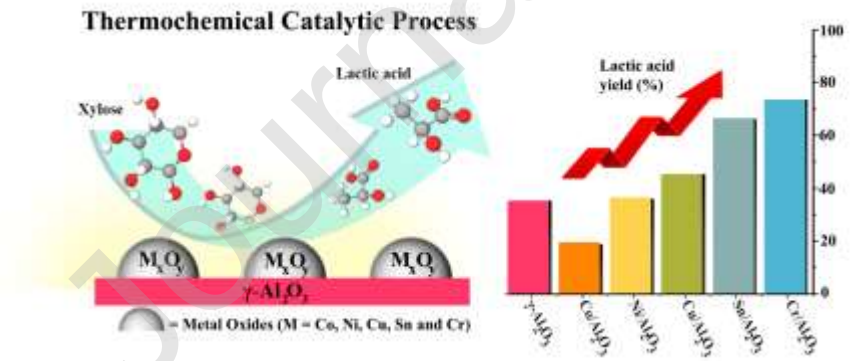

Highlights

- Deposition of Cr, Co, Cu, Ni, or Sn oxides on γ-Al_2O_3 can promote Lewis acid sites.
- The acidity of the catalysts influences the lactic yield.
- Cr/Al_2O_3 and Sn/Al_2O_3 are promising catalysts for lactic acid production.
- The low-cost catalysts are simply prepared by impregnation technique.
- Cr/Al_2O_3 and Sn/Al_2O_3 catalysts have the potential for industrial-scale application.

Abstract

Gamma-alumina (γ-Al_2O_3) is a low-cost amphoteric solid catalyst which can enhance the transformation of D-xylose into lactic acid. The deposition of metal oxides on γ-Al_2O_3 could further improve the yield of lactic acid from xylose. Therefore, in this work, the thermochemical catalytic conversion of D-xylose to lactic acid using the Cr, Cu, Co, Ni, and Sn oxides supported on γ-Al_2O_3 as heterogeneous catalysts was studied. The effects of metal oxides on the D-xylose conversion to lactic acid activity of the catalysts were investigated. It was found that, under identical testing conditions (170 °C, 4 h), Cr/Al_2O_3 is superior to the other catalysts with the 99 % conversion of D-xylose and the lactic acid yield of 74%. The outstanding activity could be attributed to its richness in Lewis-acid sites. Since the highly active Cr/Al_2O_3 catalyst is composed of the earth-abundant materials and can be prepared by a simple process, it has feasibility for industrial-scale application.

Keywords: Lactic acid; Xylose; Al_2O_3, Heterogeneous catalyst; Metal oxides.

1. Introduction

Lactic acid is one of the essential biomass-derived platform chemicals which is used in various industrial applications. For example, it is used as an acidulant and preservative agent in the food and beverage industries. The esters of lactate salts with longer chain fatty acids are used as emulsifying agents (e.g., calcium and sodium stearoyl-2-lactylate) in food and bakery goods [1]. Moreover, lactic acid is a precursor in the synthesis of several value-added chemicals, and an ingredient in the production of cosmetics, pharmaceuticals, and biodegradable polymers [1, 2]. Currently, lactic acid is mainly produced by fermentation of carbohydrates in the presence of microorganisms [2]. However, high nutrient costs, low volumetric productivities, long production periods with low space-time yields and complicate purification processes limit its upscaling production [3]. Thus, non-fermentative approaches such as thermochemical conversion of biomass with acid catalysts have increasingly received attention [4, 5].

There are a number of reports on thermochemical catalytic conversion of triose (glycerol, dihydroxyacetone and glyceraldehyde) [6] and hexose (fructose and glucose) sugars to lactic acid by Lewis acid catalysts [3, 7, 8]. However, there are only a few reports on the conversion of pentose sugars, especially xylose [9-11] which is one of the most abundant components derived from lignocellulose. For example, Takagaki et al. [12] have demonstrated that solid Lewis acid catalysts with a high content of aluminum, especially gamma-alumina (γ-Al_2O_3), could yield high selectivity of lactic acid in the transformation of C3 and C6 sugars in water. Gamma-alumina (γ-Al_2O_3) is widely used as both a Lewis acid catalyst and catalyst support in many reactions [10, 11, 13-15], due to its large surface area with bi-functional acid-base properties, high stability, and low cost.

Many metal-based Lewis acids such as tin chlorides ($SnCl_2$ and $SnCl_4$) [16, 17], copper sulfate ($CuSO_4$) [18], cobalt sulfate ($CoSO_4$) [18], nickel sulfate ($NiSO_4$) [18, 19], chromium chlorides ($CrCl_2$ and $CrCl_3$) and chromium sulfate ($Cr_2(SO_4)_3$) [20] have been reported as the active catalysts for converting sugars to lactic acid. Different types of metal cations possess different catalyst properties, such as acidity, acid site, metal-support interaction, or oxygen adsorption capacity [21]. Moreover, the deposition of metal oxides supported on γ-Al_2O_3 could further enhance the D-xylose conversion and yield of lactic acid. Therefore, the composites of γ-Al_2O_3 and metal-based Lewis acids could be potentially promising heterogeneous catalysts for the transformation of D-xylose to lactic acid. In this work, we study the effects of various metals cations dispersed on γ-Al_2O_3 support (M/Al_2O_3 where M = Co, Cu, Ni, Cr, Sn) on thermocatalytic D-xylose-to-lactic acid conversion in aqueous solution.

2. Experimental

2.1 Preparation of the metal-based Lewis acid supported on γ-Al_2O_3

γ-Al_2O_3 was prepared by calcination of boehmite, (γ-AlO(OH)), SASOL Germany GmbH) at 450 °C for 3 h under air atmosphere with a ramp rate of 5 °C/min [22]. In the typical incipient wetness impregnation, the solution of 10 wt. % of the metal precursors, including $Co(NO_3)_2 \cdot 6H_2O$ (99%, Ajax Finechem), $Cu(NO_3)_2 \cdot 3H_2O$ (99%, Ajax Finechem), $Ni(NO_3)_2 \cdot 6H_2O$ (99%, Ajax Finechem), $Cr(NO_3)_3 \cdot 9H_2O$ (99%, HIMEDIA), and $SnCl_2 \cdot 2H_2O$ (99%, Sigma Aldrich) were added dropwise on γ-Al_2O_3 under stirring. After that, the mixture was vacuum dried overnight at 60 °C. The obtained powder was then thoroughly ground and calcined at 550 °C in a muffle furnace

for 4 h with a ramp rate of 5 °C/min. The final catalysts were assigned as M/Al_2O_3 depending on the metal precursors (M = Co, Cu, Ni, Cr, Sn).

2.2 Characterization of the catalysts

The crystalline phases of γ-Al_2O_3 support and M/Al_2O_3 catalysts were characterized by X-ray diffraction (XRD) on a Bruker D8 ADVANCE with a monochromatic light source Cu K_α radiation (λ = 1.5418 Å) operated at the voltage and current of 40 kV and 40 mA, respectively. The samples were scanned at the 2θ range of $10^o < 2\theta < 80°$ with the scan speed of 0.5 s/step and the increment of 2.0 s/step.

The porosity of the samples was analyzed by nitrogen sorption on a NOVA 2000e Surface Area and Pore Size Analyzer. Before the measurement, the samples were degassed under a vacuum at 250 °C for 2 h. The specific surface area was calculated by the Brunauer-Emmett-Teller equation (BET) while the pore size distribution was determined by the Barrett-Joyner-Halenda method (BJH). The acidity of the samples was determined by ammonia temperature-programmed desorption (NH_3-TPD) on a Belcat-B equipped with a thermal conductivity detector (TCD).

Morphology of the samples was observed by scanning electron microscopy (SEM) on JOEL/JSM-6010LV operated at 20 kV. The samples were coated with gold by sputtering (Neocoater/mp-19020NCTR). Oxidation states, geometry and binding energies of the metals and metal-γ-Al_2O_3 interaction were investigated by X-ray absorption spectroscopy (XAS) and X-ray photoelectron spectroscopy (XPS) at Beamline 5.2 & 5.3 of the Synchrotron Light Research Institute, Thailand.

2.3 Evaluation of catalytic performance

A 125 ml stainless-steel batch reactor equipped with a Teflon liner (75 mL) was used as a reactor for evaluating the catalytic performance of the catalysts. Firstly, the reactor was filled with 30 mL of DI water. Then, 0.9 g of D-xylose (98%, Sigma Aldrich) was added under stirring to obtain the final concentration of 0.2 M. The desired amount of the catalysts (0.1, 0.5 and 1.0 g) was then added into the D-xylose solution with continuous magnetic stirring. After that, the reactor was sealed and purged with nitrogen gas to remove air, and then pressurized to 15 bar. The reaction was performed at the temperature range of 130-190 °C for 6 h. When the reaction was completed, the autoclave reactor was quenched in an ice bath and the solid catalyst was separated by filtration through a 0.22 µm Nylon filter membrane. The liquid product was analyzed by high performance liquid chromatography (HPLC, Shimadzu) equipped with a UV-Vis detector and a refractive index (RI) detector. Aminex HPX-87H column from Bio-Rad was employed for product analysis using 5 mM H_2SO_4 as a mobile phase with a flow rate of 0.6 mL/min at a column temperature of 45 °C. The conversion and product yield were calculated by equations 1 and 2:

$$\text{Conversion } (\%) = \left(\frac{\text{Initial mole of reactant - Final mole of reactant}}{\text{Initial mole of reactant}}\right) \times 100 \quad \text{.....(1)}$$

$$\text{Yield } (\%) = \left(\frac{[\text{P}] \times V_f \div M_W \times \text{Cpn}}{\text{Mass of xylose} \times \text{Crn atoms} \div M_W \text{ xylose}}\right) \times 100 \quad \text{.....(2)}$$

where, [P] = concentration of product from HPLC, V_f = final volume of the reaction, M_W = molecular weight of each compound, Cpn = number of carbon atoms of each product and Crn = number of carbon atoms of reactant.

3. Results and discussion

3.1 Characterization of the catalysts

3.1.1 Crystal structure and textural property

The crystalline phases of γ-Al_2O_3 and M/Al_2O_3 catalysts were characterized by powder XRD patterns as shown in Fig. 1. The diffraction pattern of Al_2O_3 is consistent with the characteristic peaks of the gamma-phase (PDF 00-001-1303). This result confirms a transformation of boehmite to γ-Al_2O_3 by calcination at 450 °C. For the metal-loaded catalysts, the characteristic peaks of γ-Al_2O_3 are still observed indicating that the gamma-phase of Al_2O_3 remained unchanged after calcination. In addition, the metal-loaded catalysts exhibit the characteristic diffraction patterns of the individual metal oxide species. Namely, the characteristic peaks of Co_3O_4 (PDF 00-043-1003), NiO (PDF 01-081-0711), SnO_2 (PDF 01-070-6153) and CuO (PDF 01-077-7716) are observed on Co/Al_2O_3, Ni/Al_2O_3, Sn/Al_2O_3, and Cu/Al_2O_3, respectively. However, there is an exception that the peaks of chromium oxides are not observed from Cr/Al_2O_3. According to the literature, $Cr(NO_3)_2 \cdot 9H_2O$ can be transformed to chromium oxide (Cr_2O_3) on γ-Al_2O_3 by calcination at 550 °C [22, 23]. In this case, the chromium oxide species may be in an amorphous phase or well dispersed on the support.

Fig. 1.

The nitrogen adsorption-desorption isotherms and pore size distribution of γ-Al_2O_3 and M/Al_2O_3 catalysts are shown in Fig. 2. The specific surface area and total pore volume are listed in Table 1. In Fig. 2A, the isotherms of all samples exhibit type IV isotherm with H1 hysteresis loop type according to the recent IUPAC classification [24]. The hysteresis loop from the condensation step at a relative pressure range of $P/P_0 = 0.6 – 0.9$ indicates the existence of non-

uniform mesopores in the samples with a regular tubular porosity. Besides, the pore sizes of all samples are similar, with the average of 7.7 nm. As indicated in Table 1, the BET surface area of as-prepared γ-Al_2O_3 (189 m^2/g) is lower than that in some other literature (230-250 m^2/g) [22, 25]. The difference might be attributed to the difference in the starting precursors. Furthermore, the BET surface areas of all M/Al_2O_3 catalysts are similar and slightly smaller than that of the γ-Al_2O_3 support. These results suggest that the addition of metal oxides has a minor effect on the textural properties of the γ-Al_2O_3 support. The comparable surface area and pore size of the metal-loaded catalysts could ensure that the catalytic performance is resulted from the metal species, not the textural properties of γ-Al_2O_3 support.

Fig. 2.

Table 1

SEM images of all samples (Fig. 3) demonstrate the unchanged morphology of γ-Al_2O_3. For all M/Al_2O_3 samples, small particles decorated on the surface of γ-Al_2O_3 with good dispersion are observed. It can be concluded that the morphology of γ-Al_2O_3 did not change after the catalyst preparation. Notably, small nanoparticles are uniformly distributed in the mesoporous channels and isolated from each other.

Fig. 3.

3.1.2 Acidic property

Surface acidic properties of γ-Al_2O_3 and various M/Al_2O_3 catalysts were investigated by ammonia temperature program desorption (NH_3-TPD) apparatus. In Fig. 4, the NH_3-TPD profile of γ-Al_2O_3 consists of three peaks around 178, 350 and 483 °C corresponding to the weak, medium and strong acid sites, respectively. Compared to the NH_3-TPD profile of γ-Al_2O_3, the intensity of the peaks representing the weak (178 °C), and medium (350 °C) acid sites are significantly increased, while the intensity of the peak representing strong acid sites (483 °C) is decreased in all cases of M/Al_2O_3 catalysts. These results indicate that the adsorbed NH_3 molecules on the surface of M/Al_2O_3 catalysts can be removed easier at the lower temperatures compared to that on γ-Al_2O_3. In other words, introducing metal oxides into γ-Al_2O_3 could increase the amount of weak acid sites and, in contrast, decrease the amount of strong acid sites. Especially, Cr/Al_2O_3 exhibited the highest amount of weak and medium acid sites, and the peak assigned to the medium acid sites is shifted to the lower temperature (~280 °C). The order of the total acidity of supported M/Al_2O_3 catalysts are Cr/Al_2O_3 > Sn/Al_2O_3 > Ni/Al_2O_3 > Cu/Al_2O_3 > Co/Al_2O_3. The involvement of the acid sites in the catalytic reaction will be discussed in the next section.

Fig. 4.

Table 2

3.1.3 Oxidation and chemical states

X-ray photoelectron spectroscopy (XPS) was employed to identify the chemical states and the elemental composition of the supported M/Al_2O_3 catalysts (Fig. 5). Fig. $5A_1$ is the XPS spectra of Co/Al_2O_3, showing two major peaks at 781.03 and 796.20 eV, which are corresponding to the Co $2p_{3/2}$ and Co $2p_{1/2}$ spin-orbit peaks of Co_3O_4, respectively [26] along with the satellite peaks at 787.59 eV and 803.24 eV. The XPS spectrum of Cr/Al_2O_3 (Fig. $5A_2$) displays two peaks at 576.82 eV and 586.71 eV which are corresponding to Cr $2p_{3/2}$ and Cr $2p_{1/2}$ of Cr^{3+}, respectively. The peaks at 579.54 eV and 588.82 eV correspond to Cr $2p_{3/2}$ and Cr $2p_{1/2}$ of Cr^{6+} [22]. These predominant peaks represented the existence of both Cr^{3+} and Cr^{6+} species on the surface of Cr/Al_2O_3. Thus, chromium oxides could be in the form of Cr_2O_3 and CrO_3. The ratio of Cr^{3+} to Cr^{6+} was 1.12 indicating that the amount Cr_2O_3 and CrO_3 on the surface are nearly the same.

In the case of supported Ni/Al_2O_3 catalyst (Fig. $5A_3$), the two main peaks at 856.87 eV and 874.56 eV correspond to Ni $2p_{3/2}$ and Ni $2p_{1/2}$. Moreover, there are shake-up satellite peaks at 862.97 eV and 880.93 eV. There are several works reported that the binding energies of Ni $2p_{3/2}$ at approximately 851.7-853 eV are attributed to Ni^0 while those at about 852.6 – 853.7 eV, 853.6 – 855.5 eV, 855.8 – 856 eV and 855.9 – 857 eV are ascribed to Al_3Ni, NiO, Ni_2O_3, and $NiAl_2O_4$, respectively [27]. The XPS and XRD results from this work confirm that the nickel oxide species of supported Ni/Al_2O_3 is NiO.

XPS spectrum of Sn/Al_2O_3 (Fig. $5A_4$) shows the two peaks with the central position at 487.38 eV and 495.85 eV, corresponding to Sn^{4+} species. According to the literature, the peaks of Sn/Al_2O_3 are from Sn with tetragonal coordination to the oxygen atoms of the host material [28, 29]. XPS spectrum of Cu/Al_2O_3 (Fig. $5A_5$) contains multi peaks corresponding to Cu $2p_{3/2}$ and Cu $2p_{1/2}$ accompanied by the satellite peaks. The peaks at 933.34 eV and 953.08 eV are the characteristics of Cu $2p_{3/2}$ and Cu $2p_{1/2}$ peaks of CuO [30]. Moreover, the small peaks at 935.32

eV and 955.32 of Cu $2p_{3/2}$ and Cu $2p_{1/2}$ are observed, suggesting the existence of $Cu(OH)_2$ in a trace amount [31]. However, the appearance of $Cu(OH)_2$ could be ascribed to water adsorption on the surface of Cu/Al_2O_3.

The O1s and Al 2p regions of γ-Al_2O_3 and supported M/Al_2O_3 catalysts were further analyzed as shown in Fig. S1 in the Supplementary Materials. The XPS spectrum of the Al_2O_3 displays the characteristic peak of O 1s and Al 2p at an approximate peak position of 531 eV and 74 eV, respectively. Comparing with the supported M/Al_2O_3 catalysts, the XPS spectrum of O 1s has a peak center in the range of 531-532 eV, while the peak centered at 74-75 eV is ascribed to Al 2p associated with γ-Al_2O_3 [32]. However, these spectra consist of two fitting peaks which could be ascribed to Al-O-Al and Al-OH species. Thus it can be noted that these peaks could be referred to various chemical compositions of Al and its hydroxyl groups, such as AlO(OH), $AlO(OH)_2$, $Al(OH)_3$ [33]. The presence of Al-OH species was due to adsorbed water.

The supported M/Al_2O_3 samples were further investigated by XANES for the information on the geometry and oxidation states. The XANES measurements were performed at the K-edge of copper, cobalt, chromium and nickel, and at the L_3-edge of Sn. The XANES results confirm that the metal species are in oxide forms. This results are in good agreement with the XRD and XPS results. Hence, it is reasonable to deduce that the dominant metal oxide species of Co/Al_2O_3, Cr/Al_2O_3, Ni/Al_2O_3, Sn/Al_2O_3, and Cu/Al_2O_3 are Co_3O_4, mixed Cr_2O_3 and CrO_3, NiO, SnO_2 and CuO, respectively.

Fig. 5.

3.2 Catalytic performance of M/Al_2O_3 for lactic acid production

3.2.1 Effects of metal oxide suppoted on γ-Al_2O_3

The supported M/Al_2O_3 catalysts and Al_2O_3 support were tested for lactic acid production from xylose at 170 °C for 6 h. The catalytic activity is shown in Fig. 6. For all catalysts, xylose conversion increases with respect to the reaction time and nearly completed (99% conversion) within 4 hours. The main product is lactic acid, and the by-products are furfural and formic acid. The order of lactic acid yields derived from M/Al_2O_3 is Cr/Al_2O_3 > Sn/Al_2O_3 > Cu/Al_2O_3 > Ni/Al_2O_3 ~ Al_2O_3 > Co/Al_2O_3. This trend is consistent with the acidity in the weak acid range. Yang et al. [11] have reported that catalytic performance of Zr-SBA-15 for the transformation of xylose to methyl lactate increases with the increasing acidity. In this work, Cr/Al_2O_3 and Sn/Al_2O_3 provide better results than the others with the yields of 74% and 66%, respectively. On the other hand, the lowest lactic acid yield is obtained from Co/Al_2O_3**,** corresponding to the lowest acidity in the weak acid range**.** It should be noted that the amount of weak acidity has an influence on the catalytic activities in our reaction condition. The reaction pathways for lactic acid production from different carbohydrate substrates seem similar.

The steps in the transformation of xylose to lactic acid in aqueous solutions are proposedand illustrated in **Scheme 1**. First, xylose undergoes retro-aldol condensation which is the breaking of C–C bond between C-2 and C-3 carbons to obtain triose species (C_3) and glycolaldehyde (C_2). The triose species could be glyceraldehyde from the retro-aldol condensation of acyclic xylose as aldopentose, and dihydroxyacetone from the retro-aldol condensation of xylulose as ketopentose from isomerization of xylose [8]. There is evidence of xylulose in our results. However, the glyceraldehyde can be isomerized to dihydroxyacetone [14] and dehydrated to 2-hydroxypropenal, then to pyruvaldehyde through keto-enol tautomerization, and finally to

lactic acid through intramolecular Cannizzaro reaction [10]. It has been discussed that the Lewis acid plays an important role in the key step of retro-aldol condensation of xylose to provide intermediates and the intramolecular Cannizzaro reaction of pyruvaldehyde to produce lactic acid selectively [10, 11, 26]. The catalytic results show that the higher lactic acid yields are obtained from the supported M/Al_2O_3 which have a higher weak acidity than the bare Al_2O_3. This indicates that the addition of Cr, Sn and Cu could enhance weak acidity which relates to the increase of lactic acid yield.

Scheme 1.

Moreover, furfural is produced via dehydration of xylose while formic acid is formed by the decomposition of glycoladehyde [10] or from the C–C splitting of pyruvaldehyde or glyceraldehyde [14] during the transformation of xylose to lactic acid.

Fig. 6.

3.2.3 Effect of reaction conditions over Cr/Al_2O_3 and Sn/Al_2O_3

The outstanding catalytic performance of Cr/Al_2O_3 and Sn/Al_2O_3 were further investigated under the temperature range of 130 to 190 °C at a reaction time of 4 hours (Fig. 7). Those catalysts show D-xylose conversion approximately 80% at 130 °C and then increase with increasing temperature up to 170 °C. At this temperature, the conversion could reach 99% and become constant at 190 °C. For lactic acid, both catalysts provide negligible yield at 130 °C. Higher yields are obtained from the higher temperature and the highest yield is obtained at 170 °C. However, the

lactic acid yield from both catalysts decrease at 190 °C because lactic acid further transforms to other small organic acids [34]. Otherwise, the small organic acids could be produced from C–C splitting of pyruvaldehyde or glyceraldehyde which are active intermediate in this reaction [14].

Fig. 7.

Furthermore, the effect of catalyst loading was also investigated on Cr/Al_2O_3 and Sn/Al_2O_3. From the results, both catalysts exhibit similar trends (Fig. 8). Catalyst loading of 0.1 g is sufficient for the complete conversion of D-xylose but the low yield of lactic acid. The high lactic acid yield is obtained with a larger amount due to more selective sites for the reaction. Similar lactic acid yield were obtained from 0.5 g and 1.0 g of catalyst. The product masses of lactic acid, furfural and formic acid with the best condition are reported in Table S4 of Supplementary Information. The best condition of 0.5g Cr/Al_2O_3 catalyst in 170 °C could provide 654 mg of lactic acid, 121 mg of furfural and 35 mg of formic acid. Thus, it can be concluded that 0.5 g catalyst is optimal for this batch reaction.

Fig. 8.

4. Conclusions

This work demonstrates an efficient alternative route for lactic acid production from D-xylose. High yields of lactic acid (~70%) at total conversion are obtained starting from D-xylose

at 170 ºC under inert conditions using the oxides of Cr and Sn supported on γ-Al_2O_3 catalysts. The results have revealed that acid sites can enhance the selectivity of lactic production. We hope that these abundant and low-cost catalysts, as well as the facile synthesis method, could have a strong potential application in an industrial scale in the future.

Credit Author Statement

1. Chanokporn Kosri : Data interpretation, Writing- Original draft preparation
2. Sirapassorn Kiatphuengporn : Writing- Reviewing and Editing
3. Teera Butburee : Writing- Reviewing and Editing
4. Saran Youngjun: XPS measuring and analysis
5. Sutarat Tongrutkaew : Experimental and interpretation
6. Kajornsak Fuangnawakij : Reviewing
7. Chakrit Yimsukanan : Data analysis and graphic design
8. Narong Chanlek : XPS analysis
9. Pinit Kijkhuntod: XAS analysis
10. Jatuporn Wittayakun : Writing- Reviewing and Editing
11. Pongtanawat Khemthong : Conceptualization, Data analysis, Writing- Reviewing and Editing

Declaration of interests

☒ The authors declare that they have no known competing financial interests or personal relationships that could have appeared to influence the work reported in this paper.

☒The authors declare the following financial interests/personal relationships which may be considered as potential competing interests:

Acknowledgements

The scholarship for C. Kosri is from the Thai government under the Development and Promotion of Science and Technology Talents (DPST) project. The authors also acknowledge support from National Nanotechnology Center (P1752682), SPAIII–Integrated Platform: Bio-based Materials (P1850012), and SUT-NANOTEC-SLRI Beamline 5.2 and 5.3 (Synchrotron Light Research Institute, Thailand) for the XANES and XPS facilities.

References

[1] R. Datta, M. Henry, Lactic acid: recent advances in products, processes and technologies — a review, Journal of Chemical Technology & Biotechnology, 81 (2006) 1119-1129.

[2] A. Komesu, J.A.R.d. Oliveira, L.H.d.S. Martins, M.R. Wolf Maciel, R. Maciel Filho, Lactic Acid Production to Purification: A Review, BioResources, 12 (2017) 4364-4383.

[3] R. De Clercq, M. Dusselier, B.F. Sels, Heterogeneous catalysis for bio-based polyester monomers from cellulosic biomass: advances, challenges and prospects, Green Chemistry, 19 (2017) 5012-5040.

[4] D.A. Cantero, L. Vaquerizo, C. Martinez, M.D. Bermejo, M.J. Cocero, Selective transformation of fructose and high fructose content biomass into lactic acid in supercritical water, Catalysis Today, 255 (2015) 80-86.

[5] J. Duo, Z. Zhang, G. Yao, Z. Huo, F. Jin, Hydrothermal conversion of glucose into lactic acid with sodium silicate as a base catalyst, Catalysis Today, 263 (2016) 112-116.

[6] R. Palacio, S. Torres, D. Lopez, D. Hernandez, Selective glycerol conversion to lactic acid on Co_3O_4/CeO_2 catalysts, Catalysis Today, 302 (2018) 196-202.

[7] R. Younas, S. Zhang, L. Zhang, G. Luo, K. Chen, L. Cao, Y. Liu, S. Hao, Lactic acid production from rice straw in alkaline hydrothermal conditions in presence of NiO nanoplates, Catalysis Today, 274 (2016) 40-48.

[8] M.S. Holm, Y.J. Pagán-Torres, S. Saravanamurugan, A. Riisager, J.A. Dumesic, E. Taarning, Sn-Beta catalysed conversion of hemicellulosic sugars, Green Chemistry, 14 (2012) 702-706.

[9] E.M. Albuquerque, L.E.P. Borges, M.A. Fraga, C. Sievers, Relationship between acid–base properties and the activity of ZrO_2-based catalysts for the Cannizzaro reaction of pyruvaldehyde to lactic acid, ChemCatChem, 9 (2017) 2675-2683.

[10] L. Yang, J. Su, S. Carl, J.G. Lynam, X. Yang, H. Lin, Catalytic conversion of hemicellulosic biomass to lactic acid in pH neutral aqueous phase media, Applied Catalysis B: Environmental, 162 (2015) 149-157.

[11] L. Yang, X. Yang, E. Tian, V. Vattipalli, W. Fan, H. Lin, Mechanistic insights into the production of methyl lactate by catalytic conversion of carbohydrates on mesoporous Zr-SBA-15, Journal of Catalysis, 333 (2016) 207-216.

[12] A. Takagaki, J.C. Jung, S. Hayashi, Solid Lewis acidity of boehmite γ-AlO(OH) and its catalytic activity for transformation of sugars in water, RSC Advances, 4 (2014) 43785-43791.

[13] A. Feliczak-Guzik, M. Sprynskyy, I. Nowak, B. Buszewski, Catalytic Isomerization of Dihydroxyacetone to Lactic Acid and Alkyl Lactates over Hierarchical Zeolites Containing Tin, Catalysts, 8 (2018).

[14] M. Xia, W. Dong, M. Gu, C. Chang, Z. Shen, Y. Zhang, Synergetic effects of bimetals in modified beta zeolite for lactic acid synthesis from biomass-derived carbohydrates, RSC Advances, 8 (2018) 8965-8975.

[15] Euzen, Alumina, Handbook of Porous Solids, 2002, pp. 1591-1677.

[16] A. Bayu, A. Yoshida, S. Karnjanakom, K. Kusakabe, X. Hao, T. Prakoso, A. Abudula, G. Guan, Catalytic conversion of biomass derivatives to lactic acid with increased selectivity in an aqueous tin(ii) chloride/choline chloride system, Green Chemistry, 20 (2018) 4112-4119.

[17] Y. Hayashi, Y. Sasaki, Tin-catalyzed conversion of trioses to alkyl lactates in alcohol solution, Chemical Communications, (2005) 2716-2718.

[18] M. Bicker, S. Endres, L. Ott, H. Vogel, Catalytical conversion of carbohydrates in subcritical water: A new chemical process for lactic acid production, Journal of Molecular Catalysis A-chemical 239 (2005) 151-157.

[19] L. Kong, G. Li, H. Wang, W. He, F. Ling, Hydrothermal catalytic conversion of biomass for lactic acid production, Journal of Chemical Technology & Biotechnology, 83 (2008) 383-388.

[20] C.B. Rasrendra, B.A. Fachri, I.G.B.N. Makertihartha, S. Adisasmito, H.J. Heeres, Catalytic Conversion of Dihydroxyacetone to Lactic Acid Using Metal Salts in Water, ChemSusChem, 4 (2011) 768-777.

[21] C.D. Evans, S.A. Kondrat, P.J. Smith, T.D. Manning, P.J. Miedziak, G.L. Brett, R.D. Armstrong, J.K. Bartley, S.H. Taylor, M.J. Rosseinsky, G.J. Hutchings, The preparation of large surface area lanthanum based perovskite supports for AuPt nanoparticles: tuning the glycerol oxidation reaction pathway by switching the perovskite B site, Faraday Discussions, 188 (2016) 427-450.

[22] Y. Wang, J. Yang, R. Gu, L. Peng, X. Guo, N. Xue, Y. Zhu, W. Ding, Crystal-Facet Effect of γ-Al_2O_3 on Supporting CrO_x for Catalytic Semihydrogenation of Acetylene, ACS Catalysis, 8 (2018) 6419-6425.

[23] M. Santhosh Kumar, N. Hammer, M. Rønning, A. Holmen, D. Chen, J.C. Walmsley, G. Øye, The nature of active chromium species in Cr-catalysts for dehydrogenation of propane: New insights by a comprehensive spectroscopic study, Journal of Catalysis, 261 (2009) 116-128.

[24] M. Thommes, K. Kaneko, V. Neimark Alexander, P. Olivier James, F. Rodriguez-Reinoso, J. Rouquerol, S.W. Sing Kenneth, Physisorption of gases, with special reference to the evaluation of surface area and pore size distribution (IUPAC Technical Report), Pure and Applied Chemistry, 2015, pp. 1051.

[25] L. Samain, A. Jaworski, M. Edén, D.M. Ladd, D.-K. Seo, F. Javier Garcia-Garcia, U. Häussermann, Structural analysis of highly porous γ-Al2O3, Journal of Solid State Chemistry, 217 (2014) 1-8.

[26] H. Zhang, Y. Hu, L. Qi, J. He, H. Li, S. Yang, Chemocatalytic Production of Lactates from Biomass-Derived Sugars, International Journal of Chemical Engineering, 2018 (2018) 18.

[27] C.Y. Li, H.J. Zhang, Z.Q. Chen, Reaction between NiO and Al2O3 in NiO/γ-Al_2O_3 catalysts probed by positronium atom, Applied Surface Science, 266 (2013) 17-21.

[28] B. Tang, W. Dai, G. Wu, N. Guan, L. Li, M. Hunger, Improved Postsynthesis Strategy to Sn-Beta Zeolites as Lewis Acid Catalysts for the Ring-Opening Hydration of Epoxides, ACS Catalysis, 4 (2014) 2801-2810.

[29] W. Dai, C. Wang, B. Tang, G. Wu, N. Guan, Z. Xie, M. Hunger, L. Li, Lewis Acid Catalysis Confined in Zeolite Cages as a Strategy for Sustainable Heterogeneous Hydration of Epoxides, ACS Catalysis, 6 (2016) 2955-2964.

[30] J. Zhou, L. Guo, X. Guo, J. Mao, S. Zhang, Selective hydrogenolysis of glycerol to propanediols on supported Cu-containing bimetallic catalysts, Green Chemistry, 12 (2010) 1835-1843.

[31] O. Akhavan, R. Azimirad, S. Safa, E. Hasani, $CuO/Cu(OH)_2$ hierarchical nanostructures as bactericidal photocatalysts, Journal of Materials Chemistry, 21 (2011) 9634-9640.

[32] B.R. Strohmeier, Gamma-Alumina (γ-Al_2O_3) by XPS, Surface Science Spectra, 3 (1994) 135-140.

[33] M. Usman, M. Arshad, S.S. Suvanam, A. Hallén, Influence of annealing environment on the ALD-Al_2O_3/4H-SiC interface studied through XPS, Journal of Physics D: Applied Physics, 51 (2018) 105111.

[34] Z. Srokol, A.-G. Bouche, A. van Estrik, R.C.J. Strik, T. Maschmeyer, J.A. Peters, Hydrothermal upgrading of biomass to biofuel; studies on some monosaccharide model compounds, Carbohydrate Research, 339 (2004) 1717-1726.

Fig.1

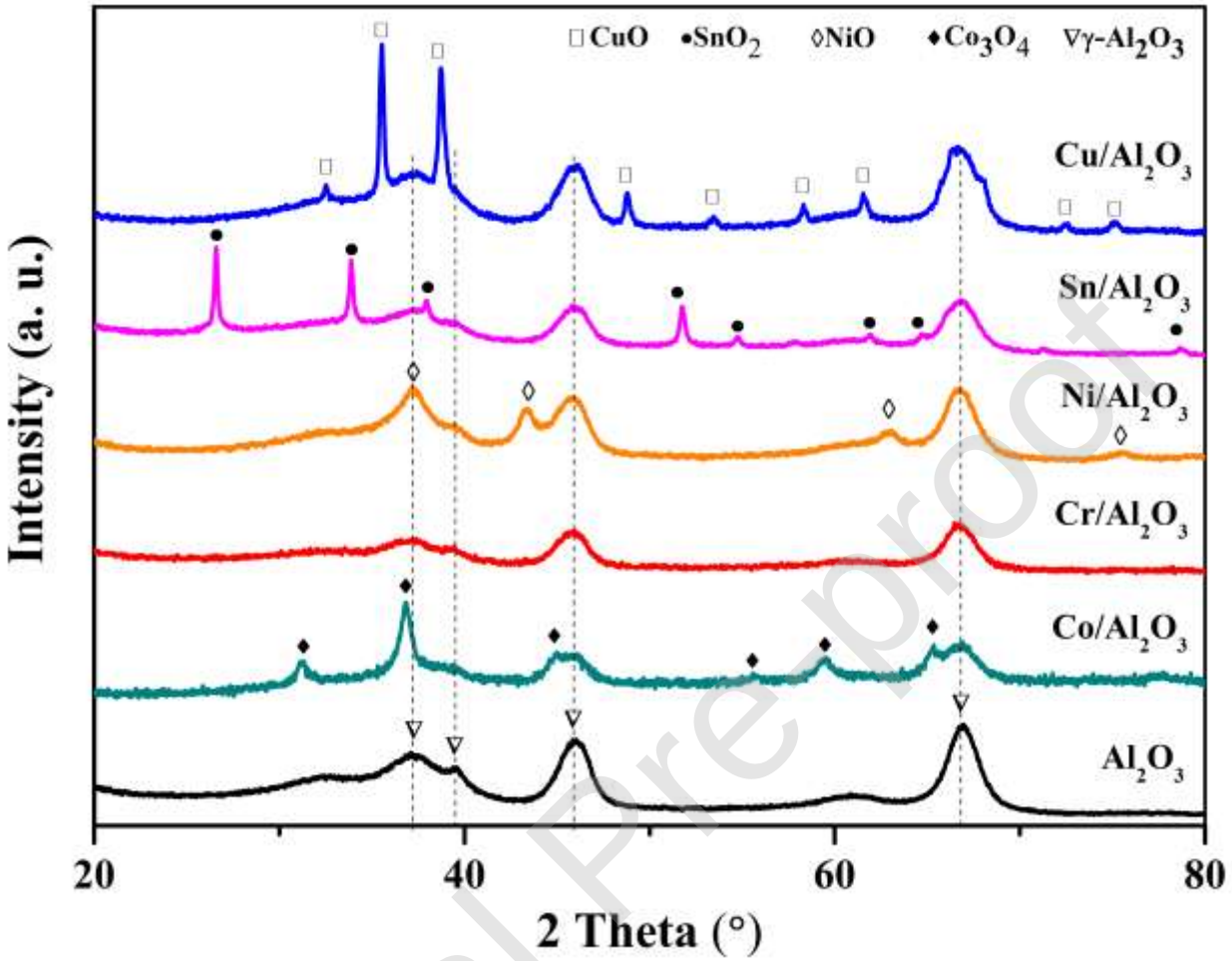

Fig.2

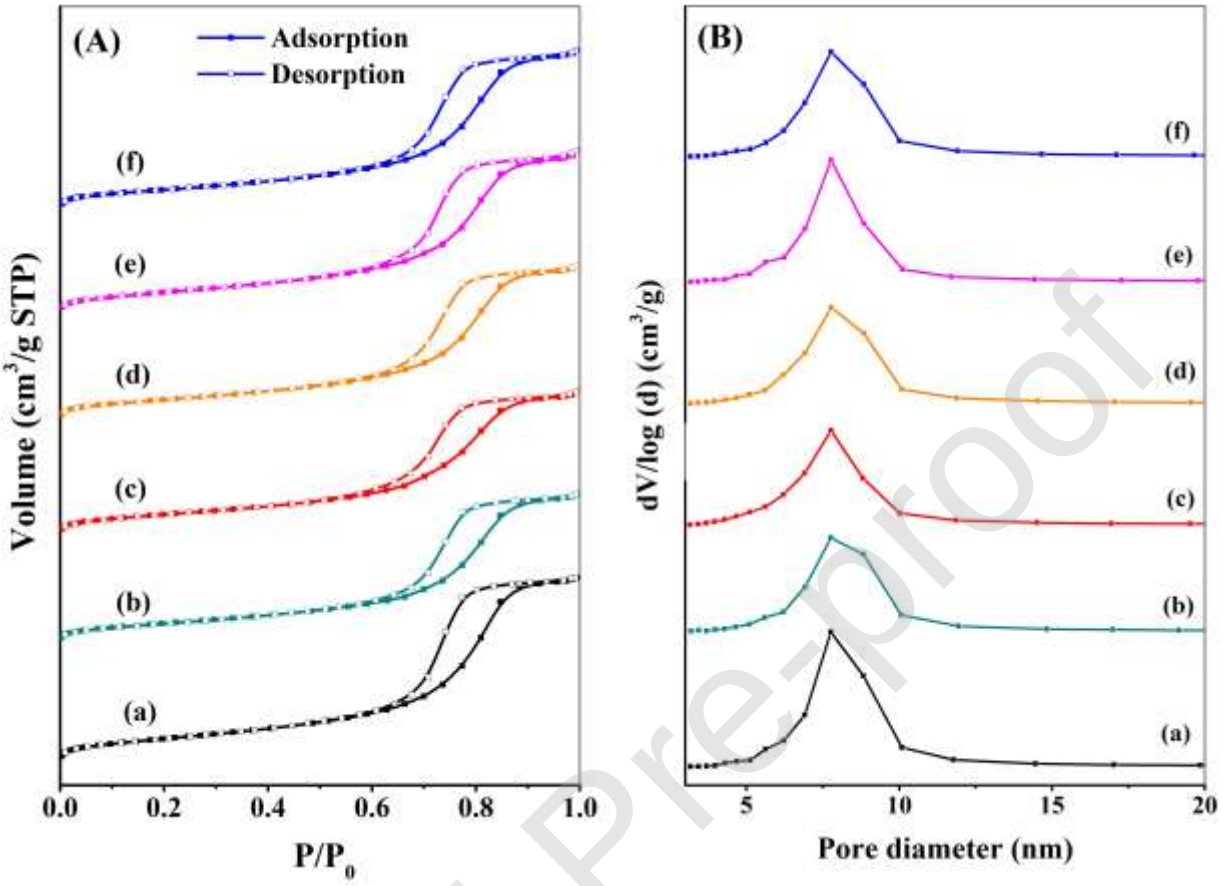

Fig.3

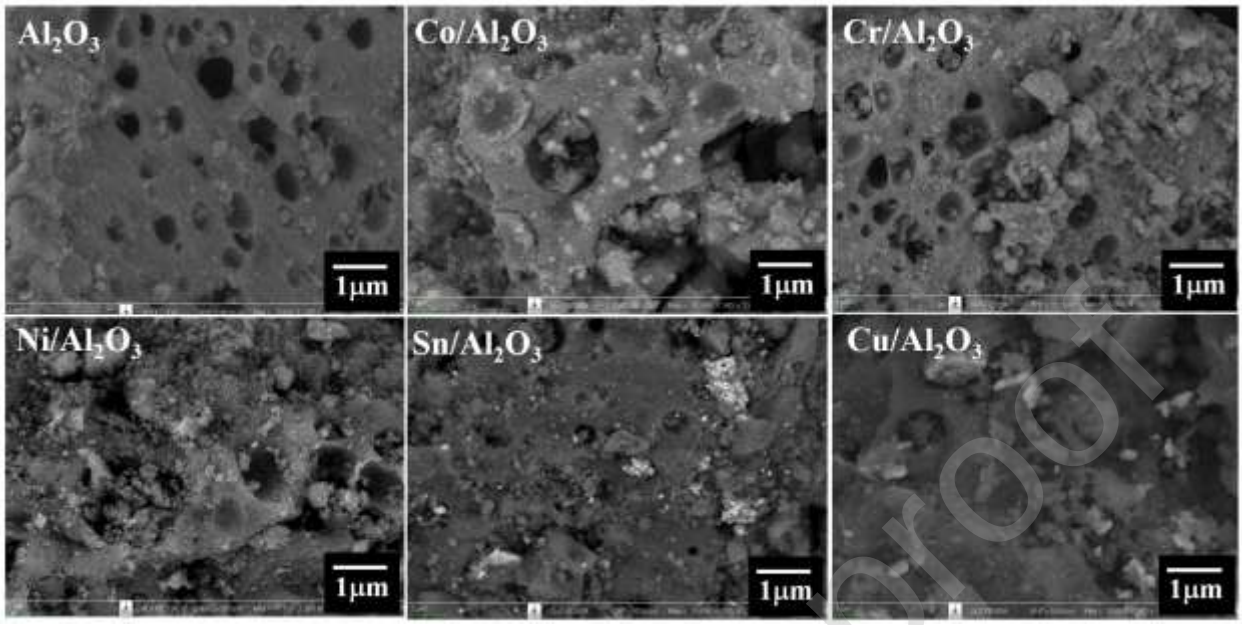

Fig.4

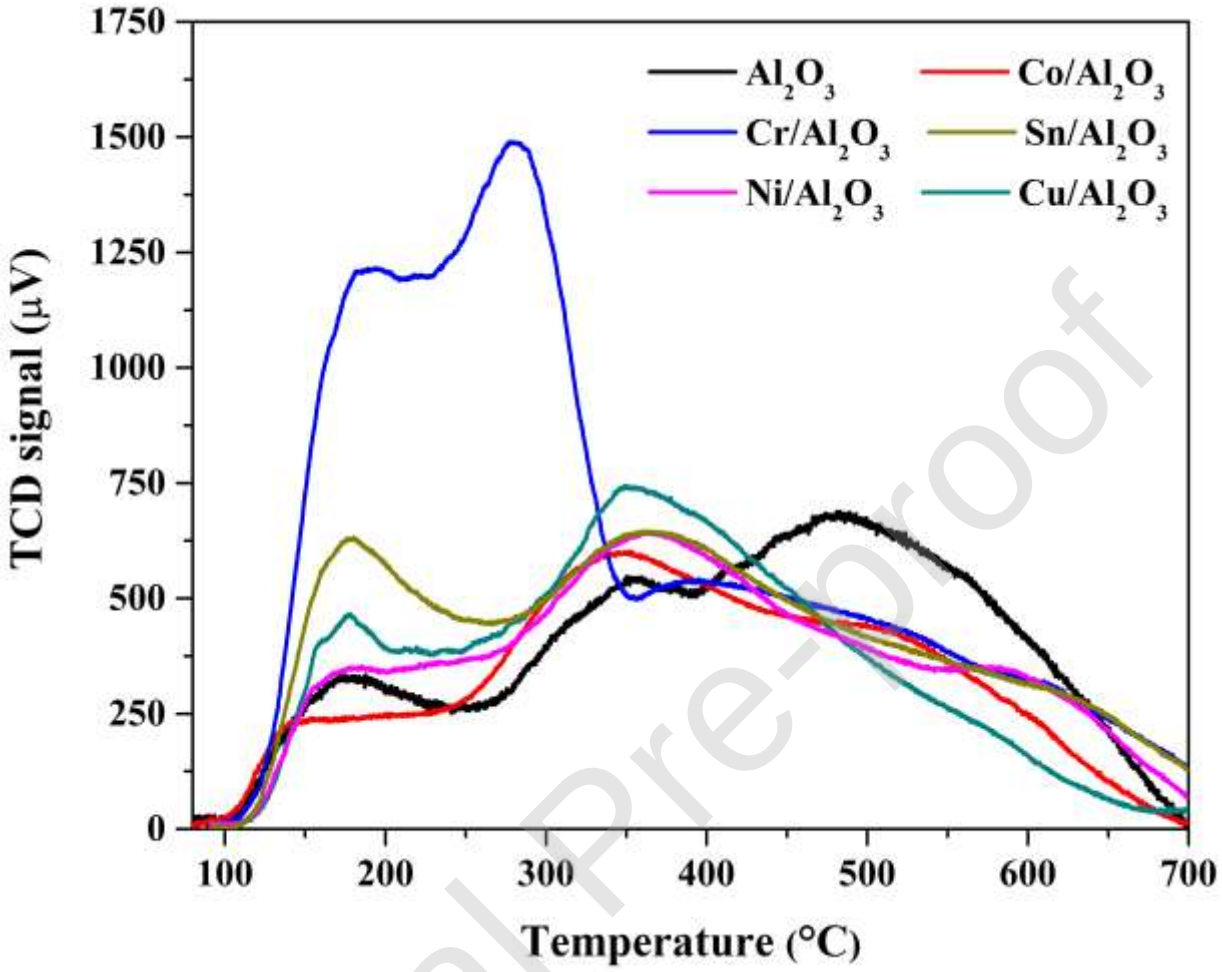

Fig.5

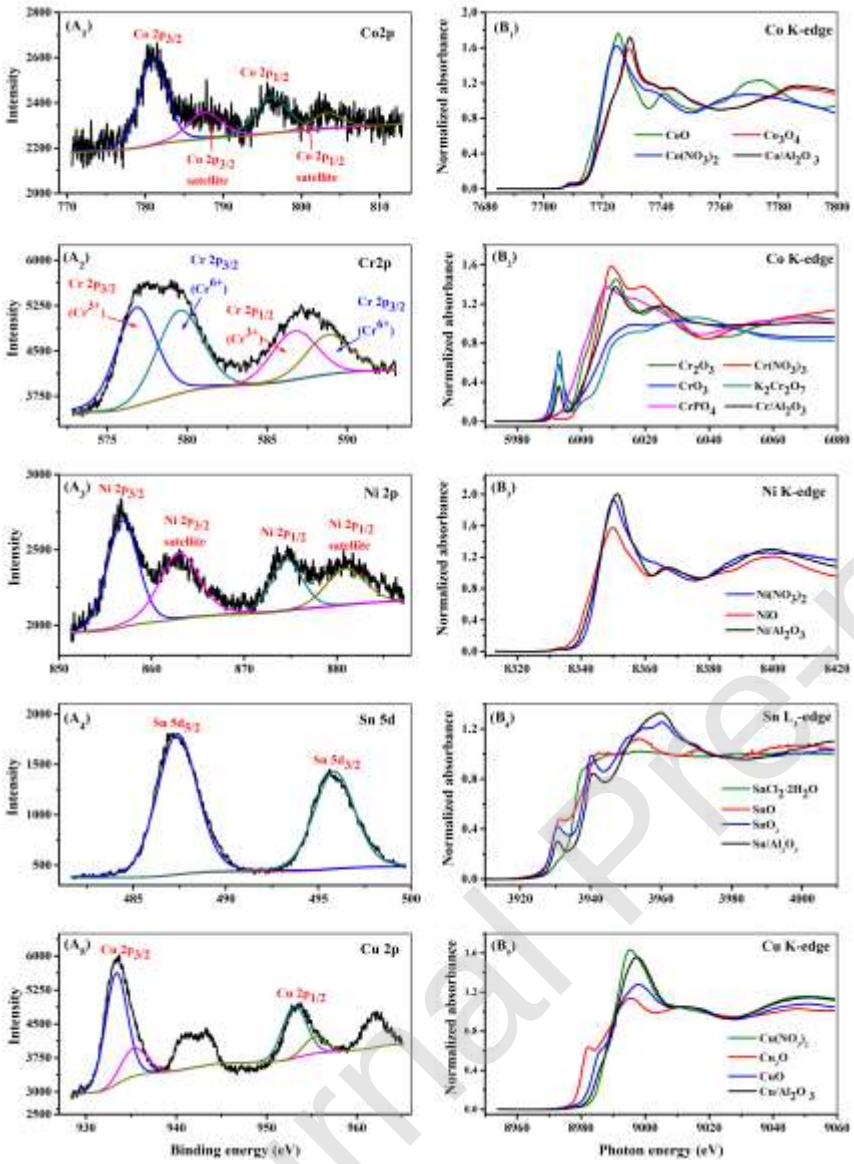

Fig.6

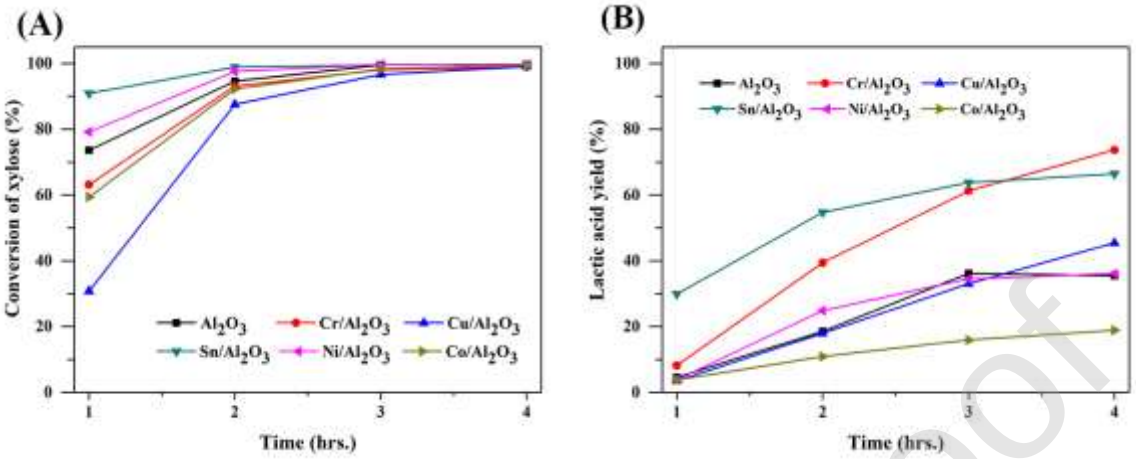

Fig.7

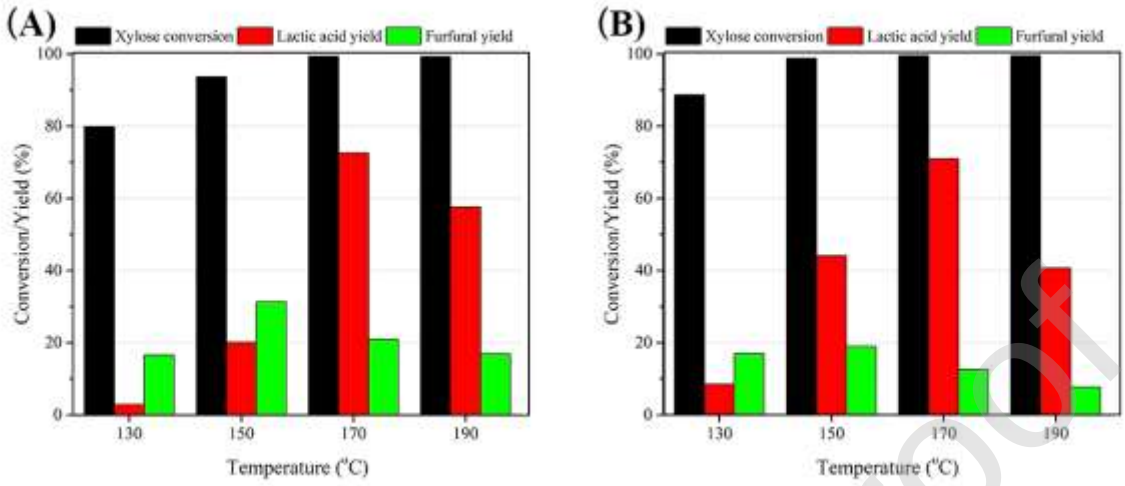

Fig.8

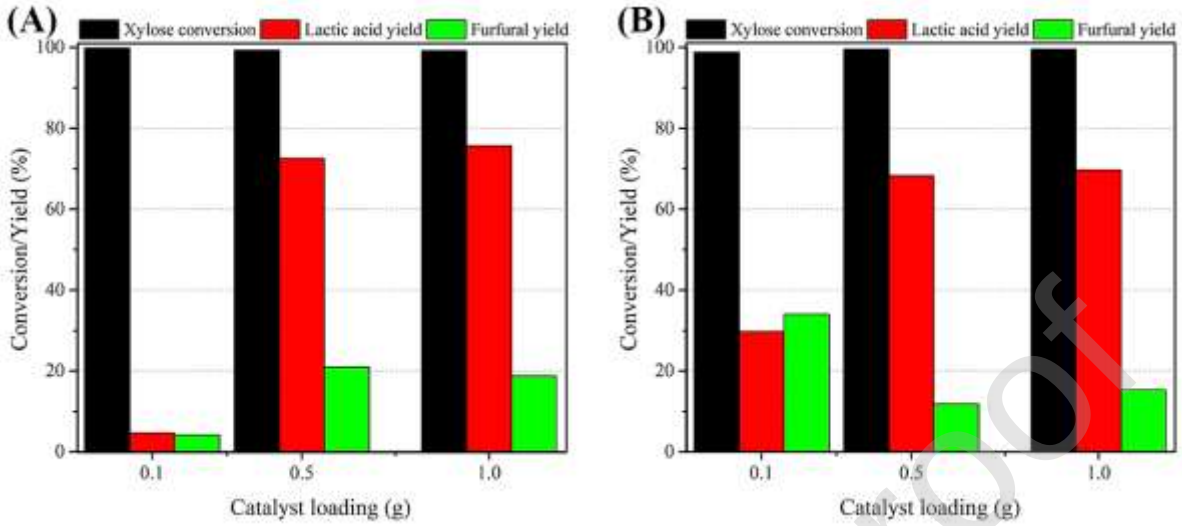

Scheme 1

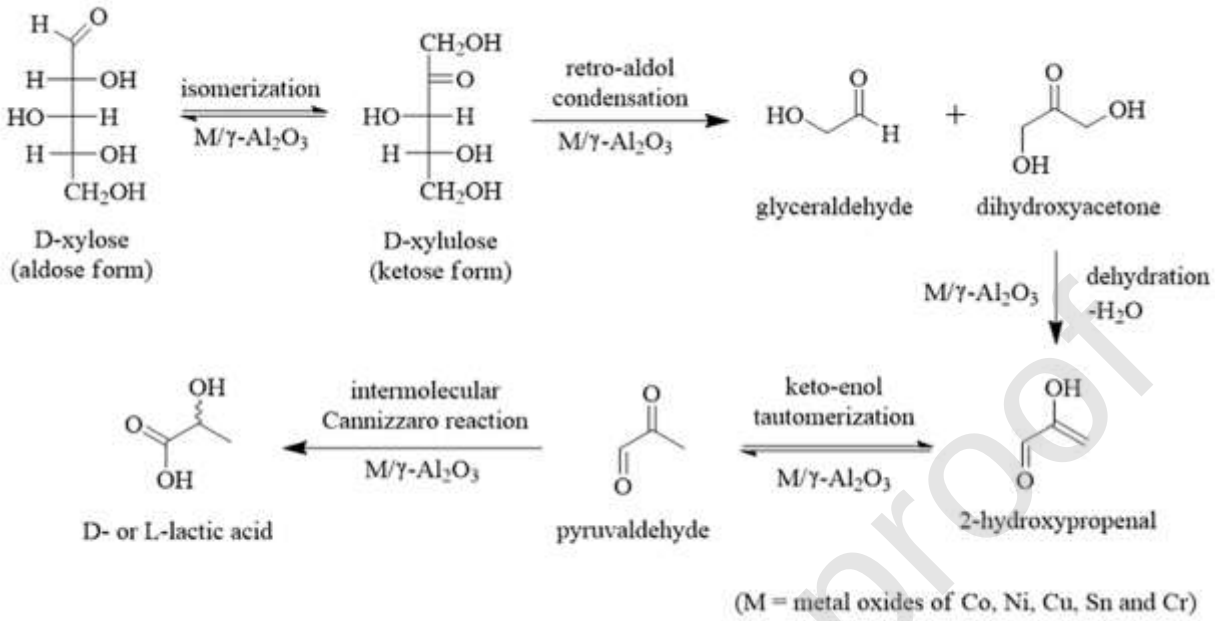

Table 1 BET specific surface area and total pore volume of γ-Al_2O_3 and supported M/Al_2O_3 catalysts.

Catalysts	BET surface area (m^2/g)	Pore Volume (mL/g)
Al_2O_3	189	0.53
Co/Al_2O_3	157	0.42
Cr/Al_2O_3	169	0.41
Ni/Al_2O_3	160	0.44
Sn/Al_2O_3	168	0.47
Cu/Al_2O_3	159	0.46

Table 2 Summary of acid properties of γ-Al_2O_3 and the supported metal-oxide catalysts: Co/Al_2O_3, Cr/Al_2O_3, Ni/Al_2O_3, Sn/Al_2O_3, and Cu/Al_2O_3.

Samples	Amount of acid				
	Acid site regions	Temperature ranges (°C)	Peak positions (°C)	Acid amount (mmol/g)	Total acid (mmol/g)
Al_2O_3	Weak	100-250	180	0.118	
	Medium	250-390	350	0.197	0.796
	Strong	390-700	490	0.481	
Co/Al_2O_3	Weak	100-220	180	0.088	
	Medium	220-450	350	0.375	0.702
	Strong	450-700	520	0.239	
Cr/Al_2O_3	Weak	100-225	180	0.320	
	Medium	225-350	280	0.483	1.305
	Strong	350-750	520	0.502	
Ni/Al_2O_3	Weak	100-250	180	0.132	
	Medium	250-530	370	0.477	0.758
	Strong	530-700	620	0.149	
Sn/Al_2O_3	Weak	100-270	180	0.215	
	Medium	250-530	370	0.453	0.847
	Strong	530-750	620	0.179	
Cu/Al_2O_3	Weak	100-240	180	0.129	0.709
	Medium	250-650	350	0.580	